Available online at www.sciencedirect.com
ScienceDirect
Applied Surface Science 253 (2006) 194–199
applied surface science
www.elsevier.com/locate/apsusc

Photoreflectance study at the micrometer scale

C. Bru-Chevallier *, H. Chouaib, A. Bakouboula, T. Benyattou

Laboratoire de Physique de la Matière, CNRS UMR 5511, INSA de Lyon, Bâtiment Blaise Pascal, 7 Avenue Jean Capelle, 69621 Villeurbanne Cedex, France

Available online 6 October 2006

Abstract

Photoreflectance (PR) spectroscopy has proven to be a very efficient non-destructive tool to get information on various semiconducting epitaxial structures as it is very sensitive to every direct optical transitions in semiconducting quantum structures and allows as well to optically measure internal electric fields in space charge layers, through Franz–Keldysh oscillation (FKO) analysis. We have developed an experimental setup to get micro-PR spectra on epitaxial structures or devices on a few micrometer size spots. Due to very low signal intensity, experimental conditions have to be very carefully controlled: the signal/noise ratio strongly depends on the pump–probe power ratio.

We give experimental micro-PR results recorded on antimonide-based heterojunction bipolar transistors (HBTs), which give the local electric field at the emitter–base junction under different biasing conditions. A second part of the paper is devoted to micro-PR analysis performed on tuneable vertical cavity surface emitting layers (VCSELs) with InP/air Bragg mirrors. In such VCSELs, both the cavity Fabry–Perot peak and the active region quantum well ground state are giving transitions in the micro-PR spectrum. This is very useful in the case of a tuneable structure. Feasibility of micro-PR analysis at the device scale is demonstrated.

Keywords: Photoreflectance spectroscopy; Micro-PR analysis; VCSELs

1. Introduction

Optical characterization at the micrometer scale is important in a wide range of science and technology. With the progress in device fabrication techniques, we need tools to characterize features whose size and separation are small, and study how reduction in size changes the physical and electronic properties of the devices. The optical characterization of devices eventually under operation is as well a very challenging subject.

The non-destructive and contactless optical characterization technique of photoreflectance (PR) [1] has been used to characterize semiconductor heterostructures and a number of device structures such as heterojunction bipolar transistors (HBTs) [2], high electron mobility transistors [3], and vertical cavity surface emitting lasers (VCSELs) [4]. PR spectroscopy allows to measure the energy gap of semiconductor alloys, direct optical transitions in quantum-confined structures, as well as electric fields in space charge layers from Franz–Keldysh analysis. Performing PR spectroscopy at the micrometer scale on a device is therefore very challenging and could open the way to a real non-destructive device characterization. Only few reports have already been published in the literature concerning micro-PR studies in laser structures [5].

After a brief description of the experimental micro-PR setup, the first part of the paper is devoted to PR spectroscopy performed at the micrometer scale on HBTs structures grown in the InP/GaAsSb material system. Antimonide alloys in the base of InP HBTs has indeed demonstrated good properties for high frequency applications [6–8]. FKO analysis will be exploited in those devices to derive local internal electric field at the emitter–base (EB) and base–collector (BC) junctions.

In the second part of the paper, PR spectroscopy is applied to analyze tuneable VCSELs with InP/air Bragg mirrors at the micrometer scale. In VCSELs epitaxial structures, we already demonstrated the interest of photoreflectance techniques for giving evidence of both the active medium optical transition as well as the cavity mode energy [4], whose matching is of a major importance to reduce the threshold current density of lasers [9]. This is even more valuable to get these information in tuneable VCSELs structures.

* Corresponding author. Tel.: +33 4 72 43 89 06; fax: +33 4 72 43 85 31.
E-mail address: Catherine.Bru-Chevallier@insa-lyon.fr
(C. Bru-Chevallier).

0169-4332/$ – see front matter © 2006 Elsevier B.V. All rights reserved.
doi:10.1016/j.apsusc.2006.05.085

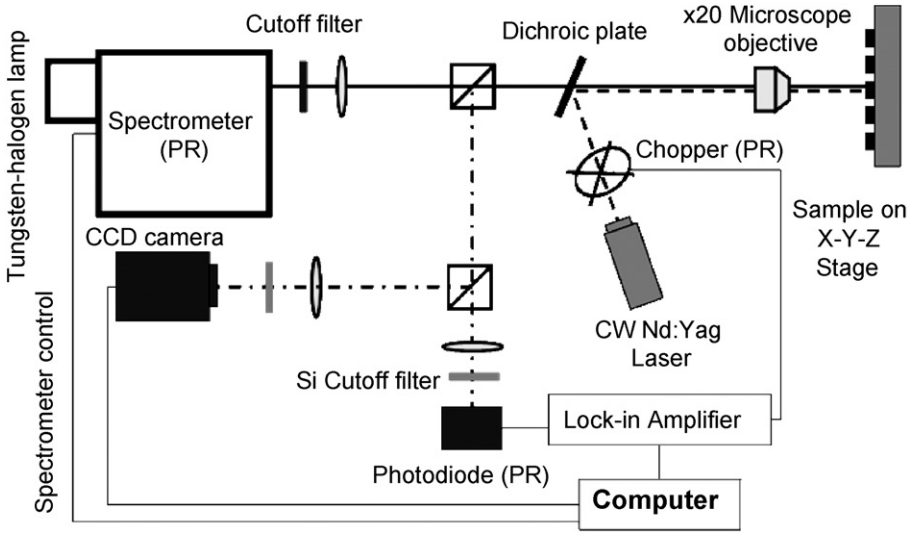

Fig. 1. Micro-PR experimental setup.

2. Experiments

As shown in Fig. 1, the probe light beam is provided from a tungsten halogen lamp which is spectrally dispersed through a spectrometer. The beam is collimated with an achromatic lens and focused on the sample using a microscope objective. A beam splitter is placed in the optical path of the light beam. It allows the collection of the reflected beam which is focused both on a photodetector for recording the PR signal and on an InGaAs CCD camera for imaging the sample. The pump light beam is provided by a laser source which is mechanically chopped and introduced in the optical path thanks to a dichroic plate. Both pump and probe beam lights are focused on the sample via the microscope objective. A long-pass filter is placed in front of the photodetector to remove the pump laser beam from the reflected signal. The modulated reflected signal is detected through a lock-in amplifier.

In PR experiments, the pump beam intensity plays a major role, as it induces a parasitic PL background which may be relatively significant even at room temperature, especially in confined systems. In order to reduce the PL parasitic signal contribution, the laser pump intensity is controlled by attenuator filters. The signal/noise ratio is shown to strongly depend on the pump–probe power ratio.

3. Micro-PR on GaAsSb/InP HBT structures

The GaAsSb/InP HBT samples were grown by molecular beam epitaxy (MBE). They consist of Si-doped InP sub-collector and collector layers ($N_{DC} = 10^{16}\,cm^{-3}$), a C-doped GaAsSb base layer ($N_{AB} = 3.6 \times 10^{19}\,cm^{-3}$), a Si-doped InGaAlAs emitter layer ($N_{DE} = 5 \times 10^{17}\,cm^{-3}$), and sub-emitter layers as well as an InGaAs contact layer. The epitaxial structure is given in Fig. 2a. Fig. 2b is a top view of a large size HBT device, showing the interelectrode spacing where micro-PR spectroscopy can be performed. The mesa edges are shown by dashed lines. The emitter contact dimensions are 75 μm × 75 μm.

In Fig. 3 is plotted the typical micro-PR spectrum recorded in a processed HBT device at room temperature under an excitation power of 0.2 mW. The excitation pump beam is provided by a HeNe laser focused by a 20× microscope objective on a spot size of 7 μm. The spectrum exhibits FKOs in two different spectral ranges, each of them corresponding to different layers in the epitaxial structure. The FKO system above 1 eV, that is above the InGaAlAs energy gap, corresponds to the local electric field arising in the InGaAlAs emitter layer at the emitter–base junction. The FKO system above 1.3 eV, that is above the InP energy gap, may correspond to different layers in the structure. Actually, it is attributed to the layer in which the electric field is supposed to be the strongest, that is the low-doped InP collector layer. It does therefore correspond to the electric field arising in the base–collector (BC) layer. The electric field values are obtained from the analysis of the FKO systems. Following the usual FKO analysis [10], energy extrema E_m in FKOs are given by:

$$m\pi = \frac{4}{3}\left(\frac{E_m - E_G}{\hbar\theta}\right)^{3/2} + \phi \quad (1)$$

where m is the extremum index, E_G the bandgap energy, E_m the PR extremum energy, ϕ is an arbitrary phase factor and $\hbar\theta = (q^2F^2\hbar^2/2\mu)^{1/3}$ is the electrooptic energy with F the electric field and μ the reduced effective mass. q and $\hbar$ are respectively the elementary charged and reduced Planck's constant.

A plot of $(4/3\pi)(E_m - E_G)^{3/2}$ *versus* index number m will yield a straight line with slope $\hbar\theta^{3/2}$ which contains the electric field F. Such a plot is reported in Fig. 4 for the FKO system arising above the InGaAlAs bandgap, that is at the EB junction. The solid line is a linear fit to Eq. (1) which yields $\hbar\theta$. Knowing the InGaAlAs bandgap energy [11] and its reduced effective mass μ, the value experimentally extracted from the FKO system is about 108.5 kV/cm (±5%) at the EB junction. A similar analysis performed on the FKO system above the InP bandgap yields the electric field value at the BC junction in this device, which is about 23.5 kV/cm (±5%).

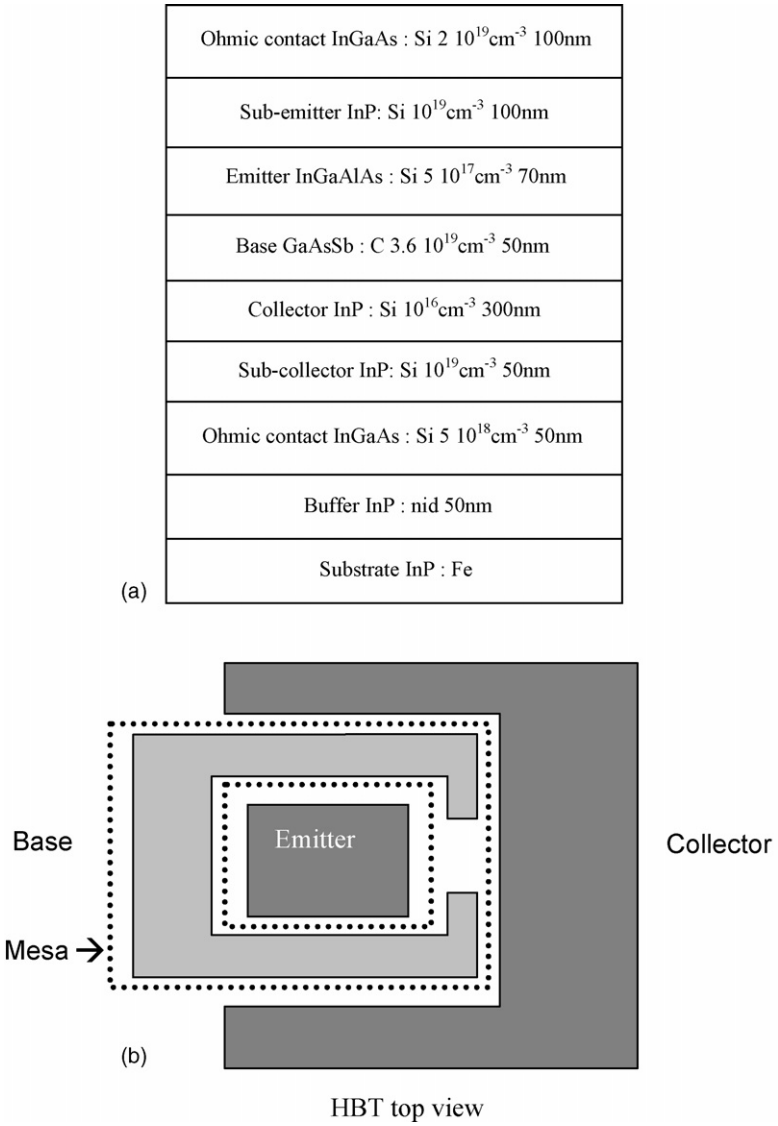

Fig. 2. Structure of the GaAsSb/InP epitaxial layer of the HBT. Top view of a processed HBT device showing emitter, base and collector metallizations. Dotted lines show the mesa edges.

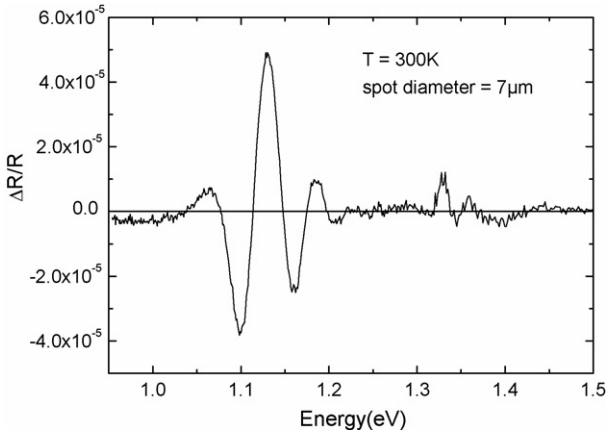

Fig. 3. Room temperature PR spectrum recorded on a HBT device on a 7 µm diameter spot on top of the emitter mesa, between emitter and base contacts.

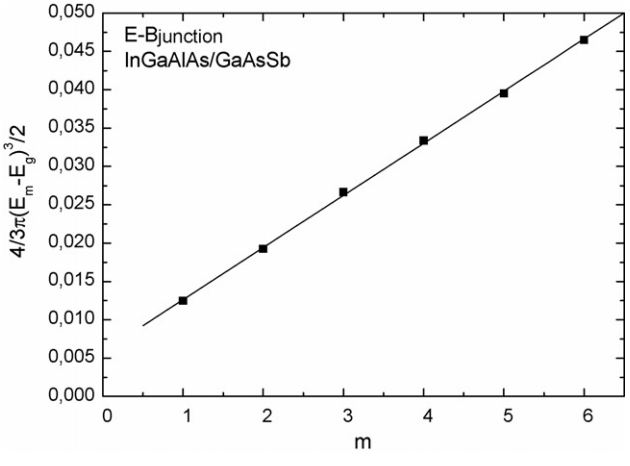

Fig. 4. Evolution of $(4/3\pi)(E_m - E_G)^{3/2}$ as a function of FKO index m in the InGaAlAs emitter layer. The solid line is a least squares fit to a linear function.

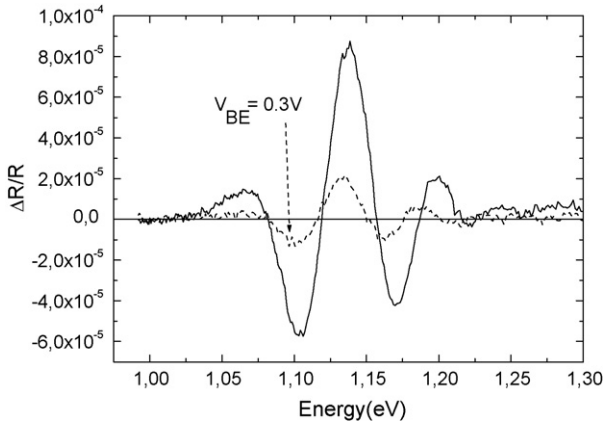

Fig. 5. Influence of emitter–base bias voltage on the FKO period in the micro-PR spectrum. The internal electric field at the EB junction is shown to decrease when the EB junction is forward biased under 0.3 V.

It is worth noting that several micro-PR spectra were recorded on different HBT devices on the same substrate, and both the PR signal intensity, and the electric field value were found to be uniform within 2% accuracy, showing the very good uniformity of growth and technology process for these devices.

The potentiality of micro-PR spectroscopy to optically measure the local electric field value is very attractive for the physical analysis of HBT operation. For this purpose, we performed again micro-PR spectroscopy on the same HBT device, under continuous biasing of the emitter–base junction. Results are plotted in Fig. 5, which shows two micro-PR spectra recorded at the same spot at top of the HBT device, with emitter–base junction either unbiased (solid line) or forward biased at 0.3 V (dashed line). The FKO system period is reduced under forward bias, showing the reduction of the internal electric field, as expected in the space charge layer of a forward biased junction. The PR intensity is also strongly decreasing in the forward biased junction.

In Fig. 6, are plotted the evolution of both the electric field value and the PR intensity as a function of biasing voltage (from reverse to forward bias). As expected, the electric field is continuously decreasing under forward bias, whereas it increases under reverse bias. Similarly, the PR intensity is decreasing as forward bias is increased. This is related to the decrease of electron–hole wavefunctions overlapping as electric field is reduced. The detailed analysis of micro-PR spectroscopy on HBT devices will soon be published [12] and further work is underway in order to get micro-PR spectroscopy on smaller size HBTs under normal bias conditions: forward biased EB junction and reverse biased BC junction.

Micro-PR spectroscopy applied to HBT devices has never been published before, and shows for the first time the very large potentiality of PR spectroscopy for the physical analysis of a such devices under operation.

4. Tuneable VCSEL devices

As previously mentioned, photoreflectance spectroscopy has already proven its efficiency in VCSELs epitaxial structures

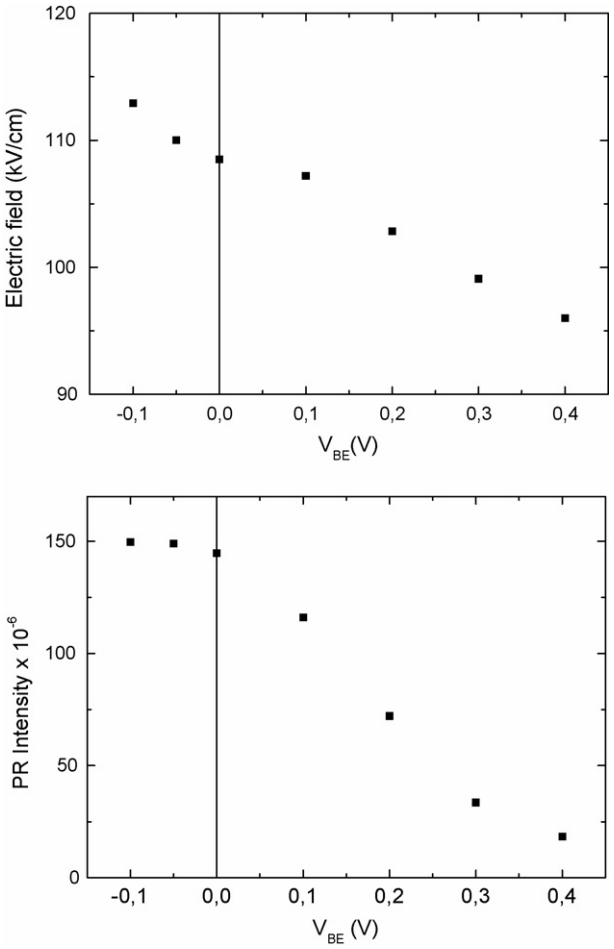

Fig. 6. Evolution of internal electric field at the EB junction *vs*. EB bias. Evolution of PR intensity *vs*. EB junction bias.

[4], as it allows to determine both active medium optical transition and Fabry–Perot cavity mode. Such parameters have to be carefully controlled in order to allow for lasing operation, and to reduce the threshold current density of laser. In the case of micromachined devices, it is well known that the residual strains can significantly change both the geometric form of structures and the Fabry–Perot mode of VCSEL cavity. Therefore, a local study such as micro-PR spectroscopy is of major importance to check for growth and microtechnology process inhomogeneities.

The studied VCSELs are a new structure, based on a bottom half VCSEL grown by metal organic chemical vapor deposition (MOCVD) and an InP/air gap micro-opto-eletromechanical system (MOEMS)-based top micromachined Bragg mirror [13]. The structure is shown in Fig. 7. Being designed as an extended distributed Bragg reflector (DBR), the bottom half VCSEL structure is thus composed by a 39.5 pair $In_{0.52}Al_{0.48}As/In_{0.53}Ga_{0.47}Al_{0.18}As$ bottom DBR and the 9λ/4-thick InP active layer in which are embedded nine $In_{0.53}Ga_{0.47}As$ quantum wells (QW) and $In_{0.62}Ga_{0.38}As_{0.82}P_{0.18}$ barriers within a 3λ/2-thick $In_{0.3}Ga_{0.7}As_{0.82}P_{0.18}$ cladding layer. As shown in the VCSEL schematic representation and in the scanning electron microscope (SEM) view of Fig. 7, the four arms suspended InP/air gap top DBR and the air gap resonant cavity

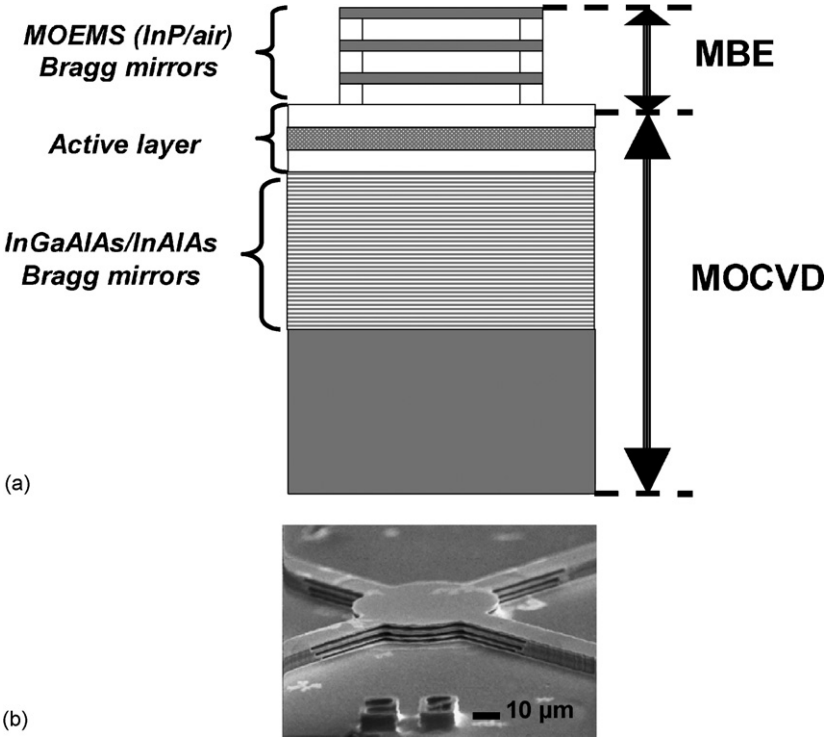

Fig. 7. (a) Schematic representation of the MOEMS VCSEL. (b) Scanning electron microscopy top view of the micromachined VCSEL.

are finally formed by reactive ion etching and selective surface micromachining of the InGaAs sacrificial layers, thus leaving an air gap between remaining InP layers. Therefore, the VCSEL structure consists of a half VCSEL and a λ/2-thick air cavity as well as a 2.5 pairs InP/air gap MOEMS-based top DBR. This structure can be electromechanically tuned thanks to an air gap on top of the cavity. Although this device is very promising, it is necessary to well control the residual strains. Actually, they can change significantly the optical properties of top DBR and air gap cavity. That is why, it is important to be able to measure the local optical properties of those devices.

Micro-PR spectroscopy was performed on one of the devices whose scanning electron microscope view is given in Fig. 7b. The excitation pump beam is provided by a 1.06 μm CW Nd:YAG laser chopped at a 180 Hz frequency with a 35 mW power, attenuated by a 0.24% neutral filter in order to reduce the parasitic PL signal which is very important in confined systems even at room temperature. The pump beam is focused at the sample surface by a 20× microscope objective on a 14 μm diameter spot. This spot diameter is well suited for the local study of the VCSEL device. Both pump and probe beams can be focused on the VCSEL structure, either at the center of free-standing membrane, or outside in order to study the bottom half VCSEL. Such experiments are expected to be a very useful tool to check for inhomogeneities in growth and technology. Indeed, the strain distribution within the free standing InP layers of the top DBR mirror of the cavity may induce large Fabry–Perot detuning among the devices which can be detrimental for laser operation.

Fig. 8 shows the micro-PR spectrum (solid line) recorded at room temperature in a complete VCSEL device, together with the micro-PR spectrum (dashed line) in the neighbor bottom half VCSEL. The half VCSEL spectrum (dashed lines) indicates a clear PR transition, which was fitted using the first derivative functional form (FDFF) of the unperturbed dielectric function, which is well-suited in the case of quantum confined systems [14]. The PR transition energy is found at 0.778 eV (1.594 μm), which corresponds to the fundamental electron–hole transition E1H1 of the active layer QWs. It falls right inside the 100 nm stop band of bottom DBR (centered at 1.605 μm). Recording such micro-PR spectra at different location on the epitaxial structure as well as on a reference active layer of the VCSEL proved a good homogeneity of the epitaxial growth.

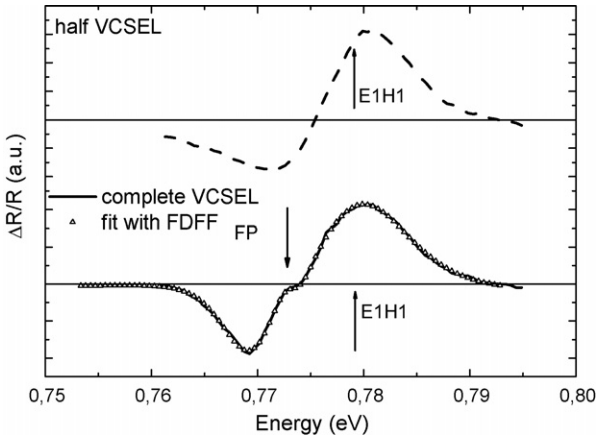

Fig. 8. Micro-PR spectrum recorded on a half VCSEL device (dashed line), a complete VCSEL structure (solid line). The fit of the PR spectrum using the first derivative functional form is plotted (triangles) for the complete VCSEL device.

Contrary to the half VCSEL spectrum, the complete VCSEL PR spectrum (solid line) exhibits a more complicated shape, as the laser cavity mode is expected to also give rise to a PR transition. Identifying the cavity mode position is a problem generally encountered in conventional PR spectroscopy of VCSEL [15]. The spatial resolution of the micro-PR technique is used here to distinguish the contribution of QW transition from Fabry–Perot cavity mode by comparing PR results on half bottom VCSEL with complete VCSEL structure. Knowing the position of the fundamental transition energy at 0.778 eV from the neighbor half VCSEL PR spectrum, the Fabry–Perot cavity mode position was deduced from complete VCSEL PR spectrum by fitting the envelop using the FDFF lineshape [14]. The fitted spectrum (triangles) is well matched to the experimental curve of the complete VCSEL device. The two PR transitions are arising, respectively, at 0.773 and 0.779 eV. The last one is attributed to the QW E1H1 transition as it is very similar in shape and energy to the transition measured in the half bottom VCSEL structure (dashed line). The second transition (0.773 eV) does correspond to the Fabry–Perot cavity mode. The detuning between QW and cavity mode is about 12 nm in the device. Such a detuning is expected to be favorable to obtain a laser effect at room temperature, following the results of Piprek et al. [16] who established a correlation between gain and cavity mode positions on lasing effect. Further results will soon be published, showing that lasing of such devices may be prevented by a too large detuning between QW and Fabry–Perot, induced either by the selective surface micromachining or by the strain distribution [17] in such tunable VCSEL devices. These results show the interest of micro-PR technique as a powerful tool to provide simultaneously QW and cavity mode energy positions directly on complete VCSEL devices.

5. Conclusion

We have applied micro-PR spectroscopy to two different kind of devices: HBT and tuneable VCSEL structures. Experimental conditions need to be carefully controlled in order to optimize the signal/noise ratio. We have shown that such a technique is efficient even on a very small spot size (a few microns) and is very useful to determine important physical parameters for device operation. In the case of HBT devices, the micro-PR spectroscopy allows to optically measure the local internal electric field at the junctions, which is of major importance in bipolar transistor operation. In tunable VCSELs, such a spectroscopic technique allows to check for devices which will not operate as a laser because of technology problems.

The feasibility of micro-PR analysis is demonstrated at the device scale. This opens the way to the local physical analysis of devices under operation.

Acknowledgements

Many thanks to Philippe Bove from Picogiga International for the growth and processing of antimonide HBTs, Jean-Luc Pelouard from LPN for fruitfull discussions about the physics of HBTs, Isabelle Sagnes from LPN for the growth of VCSEL structures and Jean-Louis Leclercq from LEOM for the VCSEL micromachining. This work was supported by the French Ministry of Research and Technology (RNRT MELBA research program), as well as by the European community (IST-1999-11051 TUNVIC research program).

References

[1] F.H. Pollak, in: M. Balkanski (Ed.), Handbook on Semiconductors, North-Holland, New York, 1994.
[2] C.J. Lin, Y.S. Huang, J. Appl. Phys. 90 (2001) 4565.
[3] H. Takeuchi, Y. Yamamoto, M. Nakayama, J. Appl. Phys. 96 (2004) 1967.
[4] P.D. Berger, C. Bru-Chevallier, T. Benyattou, G. Guillot, A. Chenevas-Paule, L. Couturier, P. Grosse, Appl. Phys. Lett. 68 (1996) 4.
[5] L. Aigouy, F.H. Pollak, G. Gumbs, Appl. Phys. Lett. 70 (1997) 2562.
[6] M.W. Dvorak, C.R. Bolognesi, O.J. Pitts, S.P. Watkins, IEEE Electron Device Lett. 22 (2001) 361.
[7] R.D. Rajavel, T. Hussain, M.C. Montes, M.W. Sawins, S. Thomas III, D.H. Chow, J. Cryst. Growth 251 (2003) 848.
[8] J. Godin, M. Riet, A. Konczykowska, P. Berdaguer, M. Kahn, P. Bove, H. Lahreche, R. Langer, M. Lijadi, F. Pardo, N. Bardou, J.-L. Pelouard, C. Maneux, M. Belhaj, B. Grandchamp, N. Labat, A. Touboul, C. Bru-Chevallier, H. Chouaib, T. Benyattou, Proceedings of the eighth European Microwave Week, October, Paris, 2005 (to be presented).
[9] S. Rapp, J. Piprek, K. Streubel, J. André, J. Wallin, IEEE J. Quantum Electron. 33 (1997) 1839.
[10] H. Shen, M. Dutta, J. Appl. Phys. 78 (1995) 2151.
[11] C.A. Wang, J.N. Walpole, L.J. Missaggia, J.P. Donnelly, H.K. Choi, Appl. Phys. Lett. 58 (1991) 2208.
[12] H. Chouaib, T. Benyattou, C. Bru-Chevallier, P. Bove, submitted for publication.
[13] J.L. Leclercq, P. Regreny, P. Viktorovitch, A. Bakouboula, T. Benyattou, I. Sagnes, G. Saint-Girons, C. Mériadec, A. Mereuta, S. Bouchoule, A. Plais, J. Jacquet, Proc. SPIE: Int. Soc. Opt. Eng. 4755 (2002) 448.
[14] Y.S. Huang, H. Qiang, F.H. Pollak, G.D. Petit, P.D. Kirchner, J.M. Woodall, H. Stragier, L.B. Sorensen, J. Appl. Phys. 70 (1991) 7537.
[15] T.E. Sale, T.J.C. Hosea, P.J.S. Thomas, IEEE Photon. Technol. Lett. 12 (2000) 1328.
[16] J. Piprek, D.I. Babic, J.E. Bowers, Appl. Phys. Lett. 68 (1996) 2630.
[17] N. Chitica, M. Strassner, J. Daleiden, Appl. Phys. Lett. 77 (2000) 202.